

Diffraction of surface wave on conducting rectangular wedge

Igor A. Kotelnikov, Vasily V. Gerasimov, Boris A. Knyazev

Novosibirsk State University, Pirogova Street 2, Novosibirsk, Russia and

Budker Institute of Nuclear Physics SB RAS,

Lavrentyeva Av. 11, Novosibirsk, Russia

Abstract

Diffraction of a surface wave on a rectangular wedge with impedance faces is studied using the Sommerfeld-Malyuzhinets technique. An analog of Landau's bypass rule in the theory of plasma waves is introduced for selection of a correct branch of the Sommerfeld integral, and the exact solution is given in terms of imaginary error function. The formula derived is valid both in the near-field and far-wave zones. It is shown that a diffracted surface wave is completely scattered into freely propagating electromagnetic waves and neither reflected nor transmitted surface waves are generated in case of bare metals which have positive real part of surface impedance. The scattered waves propagate predominantly at a grazing angle along the direction of propagation of the incident surface wave and mainly in the upper hemisphere regarding the wedge face. The profile of radiated intensity is nonmonotonic and does not resemble the surface wave profile which exponentially evanesces with the distance from the wedge face.

Comparison with experiments carried out in the terahertz spectral range at Novosibirsk free electron laser has shown a good agreement of the theory and the experiments.

PACS numbers: 42.25.Bs; 42.25.Fx; 42.25.Gy

I. INTRODUCTION

Plasmonics is now a very rapidly developing field of activity, and advancement to the mid- and far-infrared (terahertz) ranges of frequencies is one of the main streams in photonics [1, 2]. Our interest in this subject has arisen from discussions of the results of experiments on propagation of Surface Plasmon Polaritons (SPPs) along gold-ZnS-air interfaces [3], which were carried out at Novosibirsk Free Electron Laser facility [4] in the terahertz spectral range. For SPPs not to be disturbed by any material probe, plasmon-polariton characteristics were studied indirectly via sensing of the electromagnetic field in the space behind the tail facet of samples. In the experiments, the profile of radiated intensity is non-monotonic and does not resemble a surface wave profile which exponentially evanesces with the distance from the wedge face. A maximum of the radiation intensity is observed at some distance from the surface plane whereas a maximum of the surface wave field should be located at the wedge surface. These discrepancies had initiated search for theoretical explanation which has led us to the theory developed by G. D. Malyuzhinets in the 1950s.

The Sommerfeld-Malyuzhinets theory is known to provide a powerful method for exact solution to specific optical problems [5–7]. In particular, G.D. Malyuzhinets solved the problem of diffraction of a surface wave by an impedance wedge, considering it as a special case of a plane wave propagation at the Brewster angle [8]. He derived some general relations but he did not investigate the properties of integrand functions near the saddle points which is necessary for computation of the integrals. A few books and review papers [5–7] of varying elaboration provide a systematic introduction to the theory by G.D. Malyuzhinets. Some earlier approaches to the problem of diffraction by wedges and screens are reviewed in [9, 10]. We would like to add a few references to this list [11–21].

V. Zon in Ref. [9, 10] applied the Sommerfeld-Malyuzhinets technique to the diffraction of a surface wave on conducting wedge with small surface impedance but she did not succeed in obtaining the final solution. We do that in this paper. We also conclude that her calculations of the reflection and transmission coefficients for the surface wave are incorrect. To obtain correct results we introduce a sort of Landau’s bypass rule known in the theory of plasma waves [22].

In Section II, we briefly recall the properties of surface waves to a minimal extent necessary for understanding of the subsequent calculations and justify the use of the Leontovich boundary conditions at the wedge faces; in particular, we give (without derivation) a formula for the sur-

face impedance of a metal substrate coated with a thin dielectric film. The foundations of the Sommerfeld-Malyuzhinets technique are expounded in Section III. The diffracted field is calculated in Sections IV, V, and VI. A brief description of the experimental techniques and comparison of experimental results with theoretical predictions are given in Section VII. Section VIII concludes the paper and summarizes our results.

II. SURFACE PLASMONS ON A PLANE

Let a metal with the complex permittivity ε occupy the lower half-space $y < 0$. Since a TE wave (the electric field is transverse to the plane of incidence) has no surface branch, we consider a TM wave in the upper half-space $y > 0$, localized near the metal-air interface and propagating in the x -direction:

$$\begin{aligned}\mathbf{E}(\mathbf{r}, t) &= \mathbf{E}_0 \exp[-\varkappa y + i(kx - \omega t)], & \mathbf{E}_0 &= \{E_{0x}, E_{0y}, 0\}, \\ \mathbf{B}(\mathbf{r}, t) &= \mathbf{B}_0 \exp[-\varkappa y + i(kx - \omega t)], & \mathbf{B}_0 &= \{0, 0, B_{0z}\}.\end{aligned}\tag{1}$$

It is characterized by the circular frequency ω , wavenumber k , and attenuation constant \varkappa with a positive real part, $\text{Re}\varkappa > 0$. Similar fields (with a negative attenuation constant, $\text{Re}\varkappa' < 0$) could be written for the lower half-space but they are needed only for derivation of the dispersion law for the surface wave:

$$k = k_0 \sqrt{\frac{\varepsilon}{1 + \varepsilon}}.\tag{2}$$

Here

$$k_0 = \omega/c, \quad \varkappa^2 = k^2 - k_0^2,$$

the Gaussian system of units is used, and the derivation can be found elsewhere (see [23, 24]). Eq. (1) can be interpreted as an evanescent plane wave (also known as the Zenneck wave [25, 26]) propagating at a complex angle χ such that

$$k_x = k_0 \cos \chi = k, \quad k_y = -k_0 \sin \chi = i\varkappa, \quad \varkappa = ik_0 \sin \chi.\tag{3}$$

Using dispersion relation of Eq. (2) yields

$$\cos \chi = \sqrt{\frac{\varepsilon}{1 + \varepsilon}}, \quad \sin \chi = \sqrt{\frac{1}{1 + \varepsilon}}.\tag{4}$$

In a fictitious case of real ε , the surface wave exists provided that $\varepsilon < -1$. For complex values of ε there is always a solution with $\text{Im}\chi < 0$ which exponentially decreases with the distance from the

boundary of the metal. However, speaking about surface waves it makes sense only if the damping length $1/\text{Im}k_x$ is sufficiently long, i.e. $|\text{Im}k_x| \ll |\text{Re}k_x|$. This condition is certainly satisfied if $|\varepsilon| \gg 1$. Then $k_x \approx k_0(1 - 1/2\varepsilon)$ and the imaginary part of k_x is automatically small no matter how large or small the imaginary part of ε is.

Keeping the terahertz radiation at Novosibirsk Free Electron Laser [4] in mind, we will take as an example the value of permittivity

$$\varepsilon = -103260 + i310810$$

for gold at a frequency corresponding to the wavelength $\lambda = 140$ microns [27]. Then

$$\chi = 0.001022 - i0.001417,$$

$$k_x = (44880 + i0.065) \text{ m}^{-1},$$

$$\kappa = (64 + i46) \text{ m}^{-1}.$$

The components of the electric and magnetic field at the metal surface are related through the boundary condition, which can be derived from the Maxwell equation

$$\nabla \times \mathbf{B} = \frac{1}{c} \frac{\partial \mathbf{E}}{\partial t}.$$

Its x -component

$$-\kappa B_{0z} = -ik_0 E_{0x}$$

together with Eq. (3) yields the Leontovich boundary condition $E_{0x} = \sin \chi B_{0z}$. In the general case, the Leontovich boundary condition relates the tangential component of the electric field \mathbf{E}_τ with that of the magnetic field. It is usually written in the form $\mathbf{E}_\tau = \xi [\mathbf{n} \times \mathbf{B}]$, where the unit vector \mathbf{n} is directed along the outward normal to the surface of the metal, and the parameter ξ is called (dimensionless) surface impedance.

In Leontovich's theory, ξ is assumed to be a function of frequency, which depends only on the conductor material but neither on the incident angle nor the type of incident wave. Using Fresnel's formulae one can readily check that

$$\xi = \sqrt{\frac{1}{\varepsilon} - \frac{\sin^2 \theta_0}{\varepsilon^2}},$$

for a plane TM wave impinging against the metal surface under the angle θ_0 to the normal. A propagating TE wave is characterized by a different surface impedance

$$\xi = \frac{1}{\sqrt{\varepsilon - \sin^2 \theta_0}},$$

and

$$\xi = \sin \chi = \sqrt{\frac{1}{1 + \varepsilon}} \quad (5)$$

for the surface wave (1). In any case,

$$\xi \simeq 1/\sqrt{\varepsilon},$$

provided that inequation $|\varepsilon| \gg 1$ holds. We see that for large $|\varepsilon|$ the surface impedance ξ is approximately independent on parameters of the waves, which justifies using the Leontovich boundary condition on a metal surface instead of looking for complete solution for wave propagation inside a metal.

Below we will write the Leontovich boundary condition in the following form

$$\mathbf{E}_\tau = \sin \chi [\mathbf{n} \times \mathbf{B}], \quad (6)$$

assuming that the formal parameter χ is related with the surface impedance by Eq. (5). As shown above, χ can be considered as a complex angle of propagation of surface wave. For the above cited parameters of golden surface,

$$\xi = 0.00102 - i 0.00142. \quad (7)$$

Coating of metallic surfaces strongly affects the magnitude of ξ . For a metal coated with a thin film with a small width $d \ll 2\pi/k_0$ and permittivity $\varepsilon_d \gg 1$, we derived the following expression for the surface impedance:

$$\xi \simeq \frac{1}{\sqrt{\varepsilon}} - i \left(\frac{\varepsilon_d - 1}{\varepsilon_d} \right) k_0 d. \quad (8)$$

Properties of the film becomes dominating for $d \gtrsim 1/k_0 \sqrt{\varepsilon}$. For example, ZnS film with $d = 0.75\mu\text{m}$ and

$$\varepsilon_d = 8.7 + i 0.059$$

over a gold substrate has the impedance

$$\xi \simeq 0.00106 - i 0.0312 \quad (9)$$

with an imaginary part more than 20 times larger than that of pure gold.

III. SOMMERFELD-MALYUZHINETS THEORY

To begin with, let consider a plane wave of unit amplitude incident on a wedge at the angle $\theta = \theta_0 > 0$, as shown in Fig. 1. In polar coordinates r and θ perpendicular to the edge of the

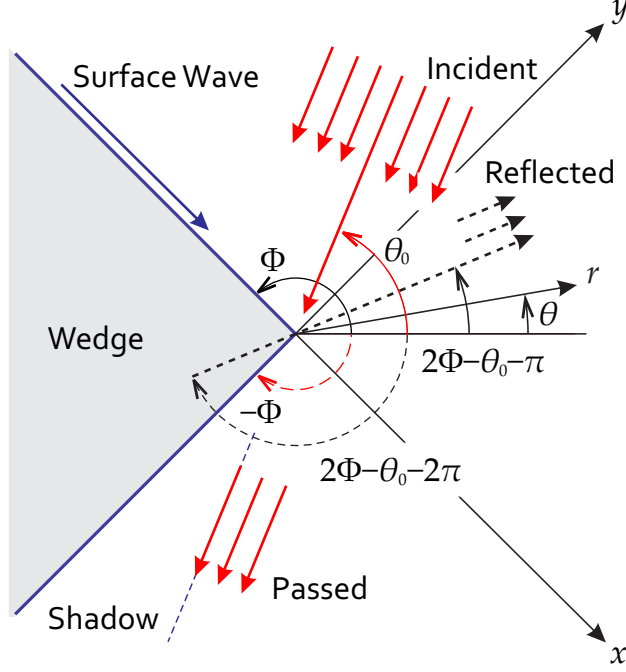


Figure 1. (color online) The geometry of the problem in cylindrical coordinates. The angles θ and Φ are measured from the bisector of the wedge.

wedge, the wave is written as

$$B_{\text{inc}} = \exp[-ik_0 r \cos(\theta - \theta_0)]. \quad (10)$$

Let the wedge occupy the region $|\theta| \geq \Phi$. Within the framework of geometrical optics, the upper face of the wedge reflects the incident wave at the angle $\theta = 2\Phi - \theta_0 - \pi$. One more π should be subtracted from this value for taking the reversal of the direction of propagation into account, thus the field of the reflected wave is derived from Eq. (10) with the substitution $\theta_0 \rightarrow 2\Phi - \theta_0 - 2\pi \rightarrow 2\Phi - \theta_0$:

$$B_{\text{refl}} \propto \exp[-ik_0 r \cos(\theta + \theta_0 - 2\Phi)]. \quad (11)$$

Below we restrict ourselves to the case of TM waves with the transversal component of magnetic field $B_z \equiv B$. The reason for such choice is that a surface wave may have no TE polarization. In the vacuum region, $|\theta| < \Phi$, the TM wave obeys the Helmholtz equation

$$\nabla^2 B + k_0^2 B = 0. \quad (12)$$

The non-zero components of the electric field in the TM wave,

$$E_r = \frac{i}{k_0 r} \frac{\partial B}{\partial \theta}, \quad E_\theta = -\frac{i}{k_0} \frac{\partial B}{\partial r}, \quad (13)$$

are expressed through the derivatives of B . The Leontovich boundary conditions in Eq. (6) with the surface impedance of Eq. (5) on the conducting faces of the wedge at $\theta = \pm\Phi$ now take the following form

$$\frac{1}{r} \frac{\partial B}{\partial \theta} = \pm ik_0 \sin \chi_{\pm} B, \quad (14)$$

where the + and – signs label the quantities related to the faces of the wedge located at the angle $\theta = +\Phi$ and $\theta = -\Phi$, respectively.

Heuristic considerations enable construction of a solution to Eq. (12) with given boundary conditions [7]. According to Sommerfeld [28], the solution is sought in the form of a superposition of plane waves

$$B(r, \theta) = \frac{1}{2\pi i} \int_{\gamma} \exp(-ik_0 r \cos p) s(\theta - p) dp, \quad (15)$$

where the integration is carried out over the contour γ in the complex p -plane, $k_0 r > 0$ and the kernel $s(\theta - p) = s(\theta - p, \theta_0, \Phi)$ is analytic outside the real axis. The shadowed areas in Figure 2 indicate the regions of the complex p -plane where $\text{Im} \cos p < 0$ and the exponent of Eq. (15) tends to zero as $kr \rightarrow \infty$.

Following Sommerfeld, we choose γ in the form of two loops. Then, the integral in Eq. (15) is a solution to Helmholtz's equation, provided that the two loops, γ_+ and γ_- , are shifted upwards and downwards correspondingly by the distance $|\text{Im}(\theta - p)| > |\text{Im}(\chi)|$; thus any singularities (see below) of the function $s(\theta - p)$ are located between these loops within the strip $-|\text{Im}(\chi)| < \text{Im}(\theta - p) < |\text{Im}(\chi)|$. Choosing the integration contour in the form of two symmetrical loops guaranties that the asymptote of the integral in Eq. (15) at $k_0 r \rightarrow \infty$ contains no converging cylindrical waves except for the incident wave of Eq. (10), and the incident wave is introduced into s through given a pole at $p = \theta_0$ as explained in [7].

Let now write functional equations for s . For the Leontovich boundary conditions of Eq. (12), we have

$$\int_{\gamma} \exp(-ik_0 r \cos p) \left[\frac{1}{r} s'(\pm\Phi - p) \pm ik_0 \sin \chi_{\pm} s(\pm\Phi - p) \right] dp = 0, \quad (16)$$

where $s' = ds/dp = -ds/d\theta$. Integrating the first term by parts yields the following equations

$$\int_{\gamma} \exp(-ik_0 r \cos p) [-\sin p \pm \sin \chi_{\pm}] s(\pm\Phi - p) dp = 0. \quad (17)$$

Since the contour $\gamma = \gamma_+ \cup \gamma_-$ consists of two loops situated symmetrically to the point $p = 0$, these equations are true if the kernel s is an even function of p . This leads us to the Malyuzhinets

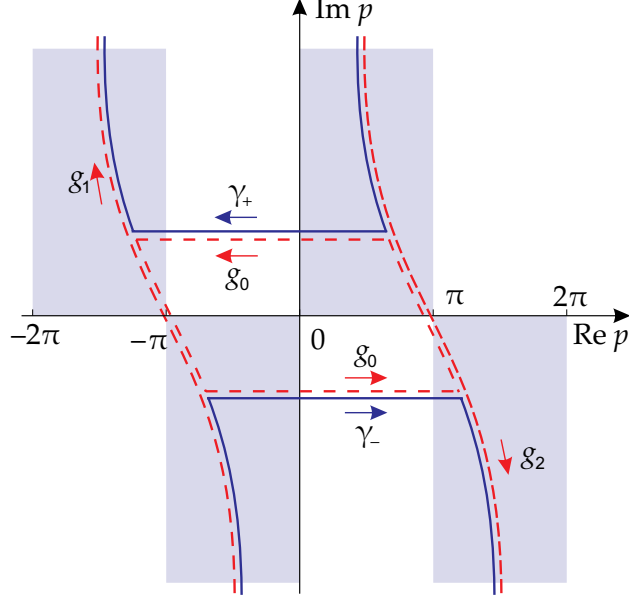


Figure 2. (color online) Plane of the complex angle p with the Sommerfeld double loops $\gamma_+ \cup \gamma_-$ (solid line) and the steepest descent paths $g_0 \cup g_1 \cup g_2$ (dashed line).

functional equations [8]:

$$\begin{aligned} [\sin p + \sin \chi_+] s(p + \Phi) &= [-\sin p + \sin \chi_+] s(-p + \Phi), \\ [\sin p - \sin \chi_-] s(p - \Phi) &= [-\sin p - \sin \chi_-] s(-p - \Phi). \end{aligned} \quad (18)$$

With rather non-trivial calculations one can verify [7] that the function

$$\Psi_0(u) = \Psi(u, \chi_+) \Psi(u - 2\Phi, \chi_-), \quad (19)$$

where

$$\Psi(v, \chi) = \psi_\Phi\left(v + \Phi + \frac{1}{2}\pi - \chi\right) \psi_\Phi\left(v + \Phi - \frac{1}{2}\pi + \chi\right), \quad (20)$$

$$\psi_\Phi(w) = \exp\left[-\frac{1}{2} \int_0^\infty \frac{\cosh(w\eta) - 1}{\eta \cosh\left(\frac{1}{2}\pi\eta\right) \sinh(2\Phi\eta)} d\eta\right], \quad (21)$$

supplies a particular solution for $s(u)$ to the functional equations (18). The Malyuzhinets function ψ_Φ is regular in the strip $|\operatorname{Re}(p)| < \frac{1}{2}\pi + 2\Phi$, where the integral in Eq. (21) is even and satisfies the following functional relation

$$\psi_\Phi(w + 2\Phi) / \psi_\Phi(w - 2\Phi) = \cot\left(\frac{1}{2}w + \frac{1}{4}\pi\right). \quad (22)$$

With Eq. (22) true this function extends beyond the indicated band.

For $\Phi = m\pi/4n$, where m/n is an irreducible rational number, the derivative $d\ln \psi_\phi/dp$ of $\ln \psi_\phi$ can be written as a finite sum of trigonometric functions [8]. In particular,

$$\psi_{3\pi/4}(w) = \frac{4}{3} \cos\left(\frac{w-\pi}{6}\right) \cos\left(\frac{w+\pi}{6}\right) \sec\left(\frac{w}{6}\right) = \frac{4}{3} \cos\left(\frac{w}{6}\right) - \frac{1}{3} \sec\left(\frac{w}{6}\right) \quad (23)$$

for $\Phi = \frac{3}{4}\pi$, which corresponds to a right angle wedge.

Looking for a general solution in the form

$$s(u) = \sigma(u)\Psi_0(u)/\Psi_0(\theta_0), \quad (24)$$

we deduce from Eqs. (18) that the function $\sigma(u)$ obeys the following equations

$$\begin{aligned} \sigma(p + \Phi) &= \sigma(-p + \Phi), \\ \sigma(p - \Phi) &= \sigma(-p - \Phi). \end{aligned} \quad (25)$$

For description of an incident wave with unit amplitude, $\sigma(\theta - p)$ should have a simple pole at $p = \theta_0$ with unit residue. By virtue of Eqs. (25), σ is symmetric about points $p = \pm\Phi$, and therefore its system of poles should satisfy the same symmetry relationships. If the pole $p = \theta_0$ is successively reflected about points $p = \Phi$ and $p = -\Phi$, one obtains for $s(\theta - p)$ a lattice of poles with the period 4Φ at $p = \theta_0 + 4n\Phi$ ($n = 0, \pm 1, \pm 2$, etc.) and a similar grid at points $p = 2\Phi - \theta_0 + 4n\Phi$. It is possible to guess a function with these properties. It was found by G.D. Malyuzhinets [29]:

$$\sigma(u) = \frac{\mu \cos(\mu\theta_0)}{\sin(\mu u) - \sin(\mu\theta_0)},$$

where $\mu = \pi/2\Phi$. For $\Phi = \frac{3}{4}\pi$

$$\sigma(u) = \frac{\frac{2}{3} \cos\left(\frac{2\theta_0}{3}\right)}{\sin\left(\frac{2u}{3}\right) - \sin\left(\frac{2\theta_0}{3}\right)}. \quad (26)$$

IV. APPROXIMATION OF GEOMETRICAL OPTICS

At a first glance, the Sommerfeld-Malyuzhinets theory might be sought of as a purely mathematical trick. However, it indeed describes a real physical phenomenon. To prove that, in this Section we show how an approximation of geometrical optics can be retrieved from this theory which provides an *exact* solution of the problem of vector field diffraction, although for a very limited set of problems related to the diffraction of electromagnetic waves on a conducting wedge. To avoid possible misunderstanding regarding the role of geometrical optics in the theory to be presented in the next three sections, it is worthy to emphasize that the field which will be derived

in the current section is merely a part of a complete solution. From mathematical point of view, it represents a contribution of the poles of the integrand core $s(\theta - p)$ in Eq. (15) whereas a complete solution (49) includes also a contribution of the saddle points $p = \pm\pi$. The separation of the contribution of the poles and saddle points can be approximately made for the distances r from the wedge top larger than the wavelength, $k_0 r \gg 1$.

Following G.D. Malyuzhinets [8], we replace the contour $\gamma = \gamma_+ \cup \gamma_-$ with the 3-loop contour $g_0 \cup g_1 \cup g_2$ shown in Fig. 2 with the dashed line, in order to compute the Sommerfeld integral in Eq. (15):

$$B(r, \theta) = \frac{1}{2\pi i} \int_{g_0 \cup g_1 \cup g_2} \exp(-ik_0 r \cos p) s(\theta - p) dp. \quad (27)$$

The contours g_0 , g_1 and g_2 are obtained by deformation of the contours γ_+ and γ_- into the steepest descent paths through the saddle points $p = -\pi$ and $p = \pi$ of the exponent $\exp(-ik_0 r \cos p)$ in the integrand. The new contour g_0 is formed from the middle parts of the contours γ_+ and γ_- , whereas the contours g_1 and g_2 are composed by remaining end parts of γ_+ and γ_- . As will be shown in Section V, the contribution of the saddle point describes the diffracted field at large distances (in the wave zone).

The integral over the contour g_0 is reduced to the sum of the residues in the poles of the integrand encircled by g_0 within the strip

$$-\pi < \text{Re}(p) < \pi. \quad (28)$$

These are the poles to be crossed during the deformation of the original contour of integration $\gamma_1 \cup \gamma_2$ to the steepest descent path contour $g_1 \cup g_2$. The number of such poles depends on the values of Φ , θ , and θ_0 .

Let consider first the poles of the function σ in Eq. (24). There are an infinite number of such poles located at the points

$$p_n = \theta - (-1)^n \theta_0 - 2n\Phi, \quad n = 0, \pm 1, \dots \quad (29)$$

However only three of them, namely

$$p_0 = \theta - \theta_0, \quad p_1 = \theta + \theta_0 - 2\Phi, \quad p_{-1} = \theta + \theta_0 + 2\Phi, \quad (30)$$

have chance to fall into the region (28) if $\Phi > \frac{1}{2}\pi$.

The residue at the pole p_0 stands for the wave $\exp[-ik_0 r \cos(\theta - \theta_0)]$, which is readily recognized as the incident wave. It enters into the result of integration if $-\pi < \theta - \theta_0 < \pi$. Values of θ outside

the interval $-\pi + \theta_0 < \theta < \pi + \theta_0$ and within the interval $-\Phi < \theta < \Phi$ represent the regions of geometrical shadow for the incident wave.

The pole p_1 gives rise to the wave $\exp[-ik_0r \cos(\theta + \theta_0 - 2\Phi)] = \exp[ik_0r \cos(\theta + \theta_0 - 2\Phi + \pi)]$, reflected from the upper face $\theta = \Phi$ of the wedge (see Fig. 1). It enters into the result of integration if $-\pi < \theta + \theta_0 - 2\Phi < \pi$, i.e. $2\Phi - \theta - \theta_0 < \pi$.

Finally, the pole p_{-1} describes the wave $\exp[-ik_0r \cos(\theta + \theta_0 + 2\Phi)]$, reflected from the lower face $\theta = -\Phi$ of the wedge. It enters into the result if $2\Phi + \theta + \theta_0 < \pi$.

Thus, the geometrical optics yields a solution constituted by ‘pieces’ of plane waves. At the ends of these pieces represented by light-shadow boundaries the solution vanishes jumpwise to zero in the shadow region, which means that the geometric-optical solution is discontinuous. These discontinuities of the optical fields will be eliminated with the addition of the diffracted fields in Section V.

The surface wave, grazing towards the wedge top along the upper face, as shown in Fig. 1, has a complex propagation angle:

$$\theta_0 = \Phi - \chi_+. \quad (31)$$

It cannot be reflected from the lower face of the wedge if $\Phi > \frac{1}{2}\pi$ as can be readily deduced from the above treatment, and only two poles, namely

$$p_0 = \theta - \Phi + \chi_+, \quad p_1 = \theta - \Phi - \chi_+, \quad (32)$$

can fall into the region given by inequation (28). This occurs if

$$\Phi - \pi \mp \text{Re}\chi_+ < \theta < \Phi, \quad (33)$$

where the upper and the lower signs stand for p_0 and p_1 , correspondingly.

Due to the factor $1/\Psi_0(\theta_0)$ in Eq. (24), the residue about the pole p_0 is evaluated as a wave of unit amplitude:

$$B_0(r, \theta) = \exp[-ik_0r \cos(\theta - \Phi + \chi_+)]. \quad (34)$$

It describes the incident surface wave propagating along the upper face to the top edge of the wedge. According to the inequation (33), this wave does not penetrate into the shadow region $\theta < \Phi - \pi$ if $\text{Re}\chi_+$ is sufficiently small. We will see in Section V that the transitional region near the formal boundary $\theta = \Phi - \pi - \text{Re}\chi_+$ of the shadow region is described by a simple function, which includes the contributions from both the pole p_0 and the saddle point $p = -\pi$.

The contribution of the pole p_1 is exactly zero, which can be seen from the fact that formally calculated residue $\Psi_0(\theta - p_1)$ contains the multiplier $\psi_\Phi(2\Phi + \pi/2)$, which is zero. Since the contributions of both the p_1 and p_{-1} poles are zero, the wedge does reflect surface waves (this assertion will be clarified in Section VI).

Let us now proceed to the poles of the function $\Psi_0(\theta - p)$. To simplify our task, below we restrict ourselves to the case of a right angle wedge with $\Phi = \frac{3}{4}\pi$. Then, $\Psi_0(\theta - p)$ is expressed through trigonometric functions with the aid of Eq. (23), and the poles can be found from the following equation

$$\begin{aligned} \cos\left[\frac{1}{6}\left(\theta - \chi_- - p - \frac{\pi}{4}\right)\right] \cos\left[\frac{1}{6}\left(\theta + \chi_- - p - \frac{5\pi}{4}\right)\right] \\ \times \cos\left[\frac{1}{6}\left(\theta - \chi_+ - p + \frac{5\pi}{4}\right)\right] \cos\left[\frac{1}{6}\left(\theta + \chi_+ - p + \frac{\pi}{4}\right)\right] = 0. \end{aligned} \quad (35)$$

They obey the conditions of Eq. (28) if

$$\begin{aligned} \frac{3}{4}\pi + \text{Re}\chi_+ < \theta \leq \frac{3}{4}\pi, \\ -\frac{3}{4}\pi \leq \theta < -\frac{3}{4}\pi - \text{Re}\chi_-. \end{aligned} \quad (36)$$

For bare metals, $\text{Re}\chi_\pm$ is positive in the optical and infrared ranges of frequencies. Hence, the inequations (36) cannot be satisfied, and the function Ψ cannot have poles inside the contour g_0 .

However the zero point

$$p_+ = \theta - \chi_+ - \frac{7}{4}\pi \quad (37)$$

of the factor $\cos\left[\frac{1}{6}\left(\theta - \chi_+ - p + \frac{5\pi}{4}\right)\right]$ approaches the first saddle point $p = -\pi$ at $\theta = \Phi = \frac{3}{4}\pi$.

Similarly, the zero point

$$p_- = \theta + \chi_- + \frac{7}{4}\pi \quad (38)$$

of the multiplier $\cos\left[\frac{1}{6}\left(\theta + \chi_- - p - \frac{5\pi}{4}\right)\right]$ is located near the second saddle point $p = +\pi$ at $\theta = -\frac{3}{4}\pi$. Although one might expect that these poles strongly affect the diffracted field near the wedge faces at $\theta = \pm\frac{3}{4}\pi$, calculations in Section VI do not confirm these fears.

V. DIFFRACTED FIELDS

Evaluating the integral in Eq. (27) along the contours g_1 and g_2 in Fig. 2 yields radiated (freely propagating) electromagnetic fields. Those contours pass through the saddle points $p = -\pi$ and

$p = \pi$, respectively. To use the saddle-point method of integration, we expand the exponent in the integrand of Eq. (27) about the saddle points so that

$$p = \mp\pi + \frac{1-i}{\sqrt{k_0 r}} t.$$

Putting the expansion

$$\exp(-ik_0 r \cos p) \simeq \exp[ik_0 r - t^2]$$

in Eq. (27) reveals that, due to the factor $\exp(-t^2)$, the main contribution to the integral over the contours g_1 and g_2 comes from the neighborhood of the saddle points. Turning to the integration in the variable t and taking into consideration the direction of integration over the contours g_1 and g_2 , we transform the respective integrals to the following form:

$$B_1(r, \theta) = \frac{1}{2\pi i} \int_{g_1} s(\theta - p) e^{-ik_0 r \cos p} dp = -\frac{1}{2\pi i} \int_{-\infty}^{\infty} s\left(\theta + \pi - \frac{1-i}{\sqrt{k_0 r}} t\right) e^{ik_0 r - t^2} \frac{dp}{dt} dt, \quad (39a)$$

$$B_2(r, \theta) = \frac{1}{2\pi i} \int_{g_2} s(\theta - p) e^{-ik_0 r \cos p} dp = +\frac{1}{2\pi i} \int_{-\infty}^{\infty} s\left(\theta - \pi - \frac{1-i}{\sqrt{k_0 r}} t\right) e^{ik_0 r - t^2} \frac{dp}{dt} dt. \quad (39b)$$

In the wave zone that corresponds to the limit $k_0 r \rightarrow \infty$, the pre-exponential factor $s(\theta - p)$ can be substituted with $s(\theta \pm \pi)$, which yields

$$B_1(r, \theta) = \frac{e^{ik_0 r + i\pi/4}}{\sqrt{2\pi k_0 r}} s(\theta + \pi), \quad (40)$$

for the contour g_1 and

$$B_2(r, \theta) = -\frac{e^{ik_0 r + i\pi/4}}{\sqrt{2\pi k_0 r}} s(\theta - \pi) \quad (41)$$

for the contour g_2 .

Since the pole $p_0 = \theta - \frac{3}{4}\pi + \chi_+$ approaches the saddle point $p = -\pi$ when θ tends to $-\frac{1}{4}\pi$, the function $s(\theta + \pi)$ has a narrow peak near $\theta = -\frac{1}{4}\pi$, which is much bigger than $s(\theta - \pi)$ as shown in Fig. 3. Hence, the field B_2 can be neglected near the peak, where the amplitude of the diffracted field is

$$B_1 \simeq \frac{1}{\sqrt{2\pi k_0 r}} \frac{\exp\left(ik_0 r + \frac{1}{4}i\pi\right)}{\theta + \frac{1}{4}\pi + \chi_+}. \quad (42)$$

The angular distribution of the intensity of the radiation field in Eq. (42) has the Lorentzian profile with the halfwidth

$$\Delta\theta = |\text{Im}\chi_+|. \quad (43)$$

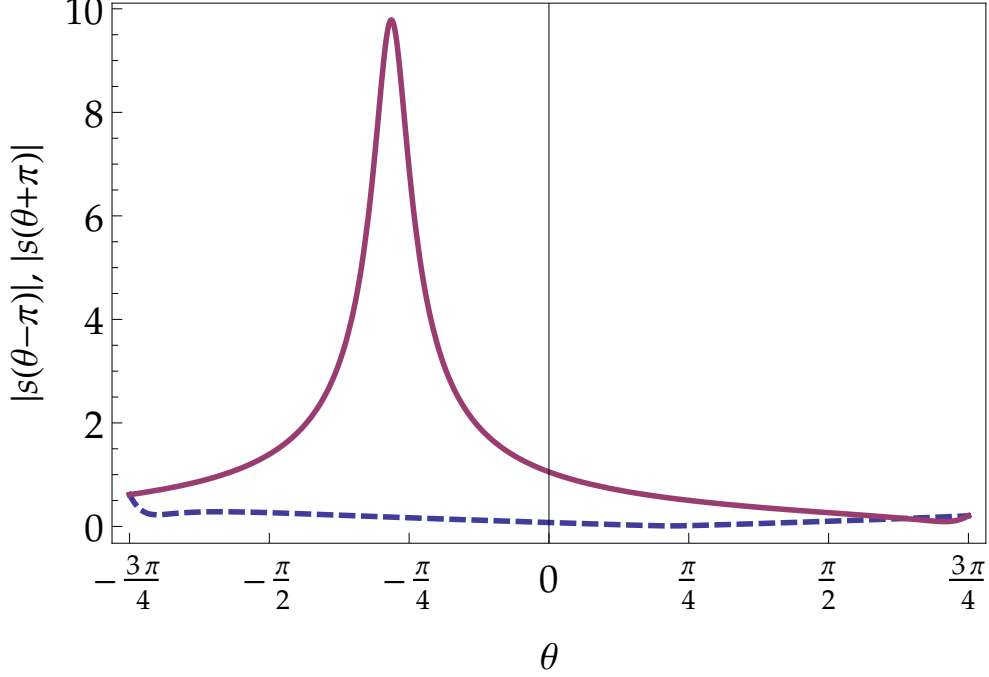


Figure 3. (color online) Functions $|s(\theta + \pi)|$ (solid line) and $|s(\theta - \pi)|$ (dashed line) for $\chi_{\pm} = 0.1(1 - i)$. The width of the narrow peak at $\theta = -\frac{\pi}{4}$ in the plot of $|s(\theta + \pi)|$ is of the order of $\text{Im}\chi_{+}$. For values of χ_{+} relevant to the THz range of frequencies, the peak is much narrower and higher.

Similar calculations were done by V. Zon in [9, 10]. Note, however, that the range of applicability of Eqs. (40)–(42) is limited to very large distances, such as

$$k_0 r \gg |\text{Im}\chi_{+}|^{-2} \simeq |\varepsilon|. \quad (44)$$

For smaller distances, the factor $s(\theta - p)$ in Eqs. (39) cannot be considered smooth as compared with the exponent $\exp(-t^2)$ since the former has a pole at $p_0 = \theta - \frac{3}{4}\pi + \chi_{+}$, which approaches the saddle point $p = -\pi$ at $\theta = -\frac{1}{4}\pi$. The absolute magnitudes of the functions $s(\theta \pm \pi)$ are plotted in Fig. 3. More accurate calculation can be performed using the following approximate expression for the kernel function

$$s(\theta - p) \simeq s_0(\theta - p) = \frac{1}{\theta - \frac{3}{4}\pi + \chi_{+} - p}. \quad (45)$$

It is derived by expanding $s(\theta - p)$ in the Laurent series about the pole p_0 but it provides a good approximation for $s(\theta - p)$ in the entire range of integration as Fig. 4 proves. Putting $s_0(\theta - p)$ in Eq. (39) yields

$$B_1(r, \theta) = \frac{1}{2\pi i} \int_{g_1} s(\theta - p) e^{ik_0 r - t^2} dp = -\frac{e^{ik_0 r}}{2\pi i} \int_{-\infty}^{\infty} \frac{\exp(-t^2)}{z_0 - t} dt, \quad (46)$$

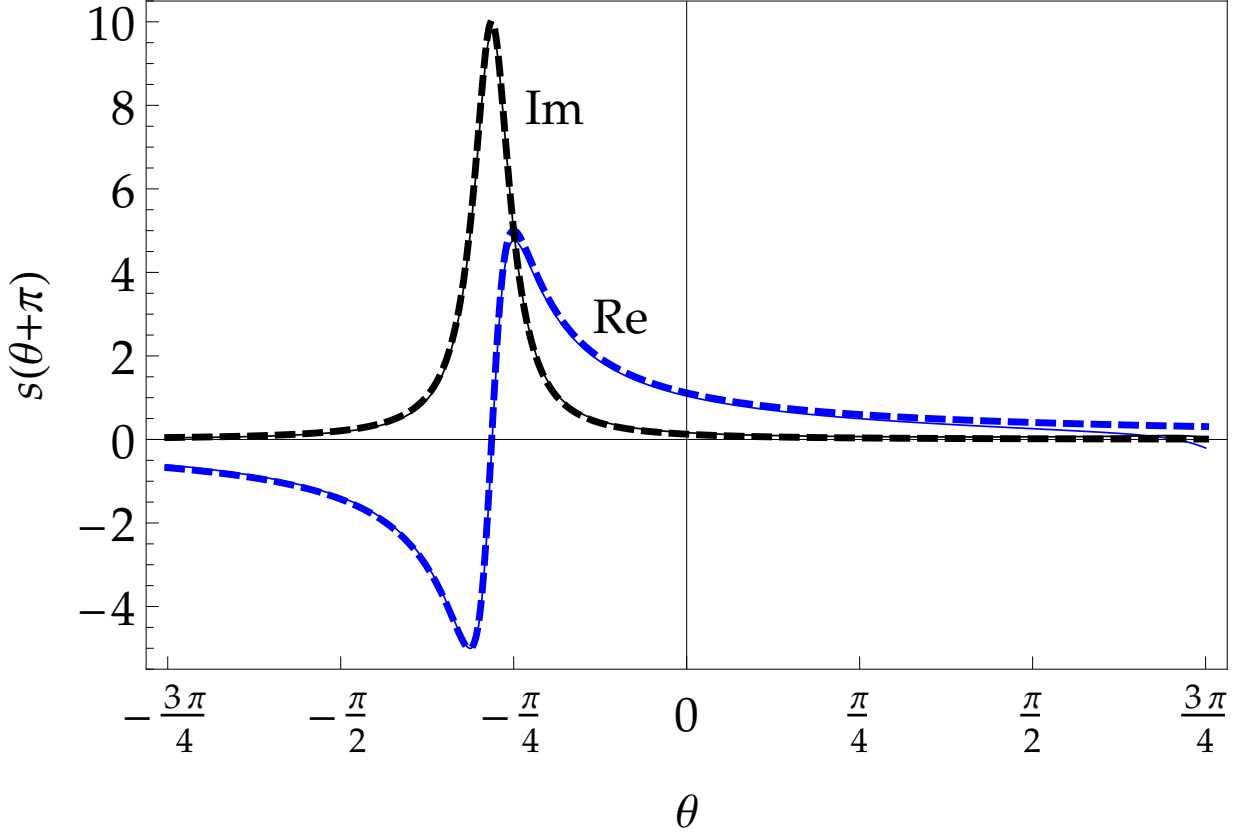


Figure 4. (color online) Comparison of $s(\theta + \pi)$ (solid line) and Laurent expansion $s_0(\theta + \pi)$ (dashed line); the real part is blue, the imaginary is black; $\chi_+ = 0.1(1 - i)$.

where

$$z_0 = \frac{\sqrt{k_0 r}}{1 - i} (p_0 + \pi) = \frac{1 + i}{2} \left(\theta + \frac{\pi}{4} + \chi_+ \right) \sqrt{k_0 r}.$$

A method of calculating the integral

$$W(z) = \frac{1}{2\pi i} \int_{-\infty}^{\infty} \frac{\exp(-t^2)}{z - t} dt \quad (47)$$

in Eq. (46) is elaborated in the theory of plasma waves [22]. The result is expressed in terms of the imaginary error function

$$\operatorname{erfi}(z) = \frac{2}{\sqrt{\pi}} \int_0^z \exp(x^2) dx$$

and has two branches:

$$W_{\pm}(z) = -\frac{1}{2} \exp(-z^2) [\pm 1 + i \operatorname{erfi}(z)]. \quad (48)$$

The first branch $W_+(z)$ is originally computed in the assumption that the imaginary part of z is positive, $\operatorname{Im}(z) > 0$, and then analytically continued to the lower half of the complex plane z , where

$\text{Im}(z) < 0$, using Eq. (48). The second branch $W_-(z)$, on the contrary, is originally computed for $\text{Im}(z) < 0$ and then analytically continued to $\text{Im}(z) > 0$. In terms of the contour integration in Eq. (47), the analytical continuation implies that the pole $t = z$ never crosses the contour of the integration (which originally goes along the axis $\text{Im}(t) = 0$), and the contour is deformed when the pole $t = z$ crosses the axis $\text{Im}(t) = 0$ to bypass the pole. Since the pole can be bypassed either from above or from below, there appear two branches of the function $W(z)$. They differ in the residue of the integrand at the pole $t = z$:

$$W_+(z) - W_-(z) = -\exp(-z^2) = \frac{1}{2\pi i} \oint_{|t-z|=\delta} \frac{\exp(-t^2)}{z-t} dt.$$

For large $|z| \gg 1$, the functions $W_{\pm}(z)$ are evaluated as

$$W_+ \approx \frac{1}{2\sqrt{\pi iz}}, \quad \text{and} \quad W_- \approx \frac{1}{2\sqrt{\pi iz}} + \exp(-z^2),$$

respectively, if $\text{Im}(z) > 0$ and as

$$W_+ \approx \frac{1}{2\sqrt{\pi iz}} - \exp(-z^2), \quad \text{and} \quad W_- \approx \frac{1}{2\sqrt{\pi iz}},$$

if $\text{Im}(z) < 0$. Note that the exponent $\exp(-z^2)$ becomes very big in sectors where $\frac{1}{4}\pi < |\arg(z)| < \frac{3}{4}\pi$.

The sign of $\text{Im}(z_0)$ is reversed as the observation point at the angle θ crosses the boundary $\theta \approx -\frac{1}{4}\pi$ of the shadow region. Together with the discontinuous field B_0 , which represents the contribution of Eq. (34) of the pole p_0 in the approximation of geometrical optics, the diffracted field B_1 forms a continuous field. This total continuous field is given by the integral of Eq. (47) in Eq. (46) computed for $\text{Im}(z) < 0$. Indeed, the pole p_0 goes away from the interior of the contour g_0 through the contour g_1 if the angle θ takes a sufficiently large negative value (which corresponds to a deep shadow region) thus making $\text{Im}(z) < 0$. In that case, the integral over the contour g_0 gives no contribution to the result of calculations so B_1 stands for the total field. Taking the lower sign in Eq. (48), we obtain the final expression

$$B(r, \theta) = -W_- \left(\frac{1+i}{2} \left(\theta + \frac{\pi}{4} + \chi_+ \right) \sqrt{k_0 r} \right) e^{ik_0 r} \quad (49)$$

for the radiation field in the proximity of $\theta = -\frac{1}{4}\pi$. In plasma physics, our choice of the branch $W_-(z)$ of the multivalued function $W(z)$ is known as the Landau rule [22]. By analytic continuation, Eq. (49) represents the total field for any values of θ . It is valid for any r larger than the wavelength

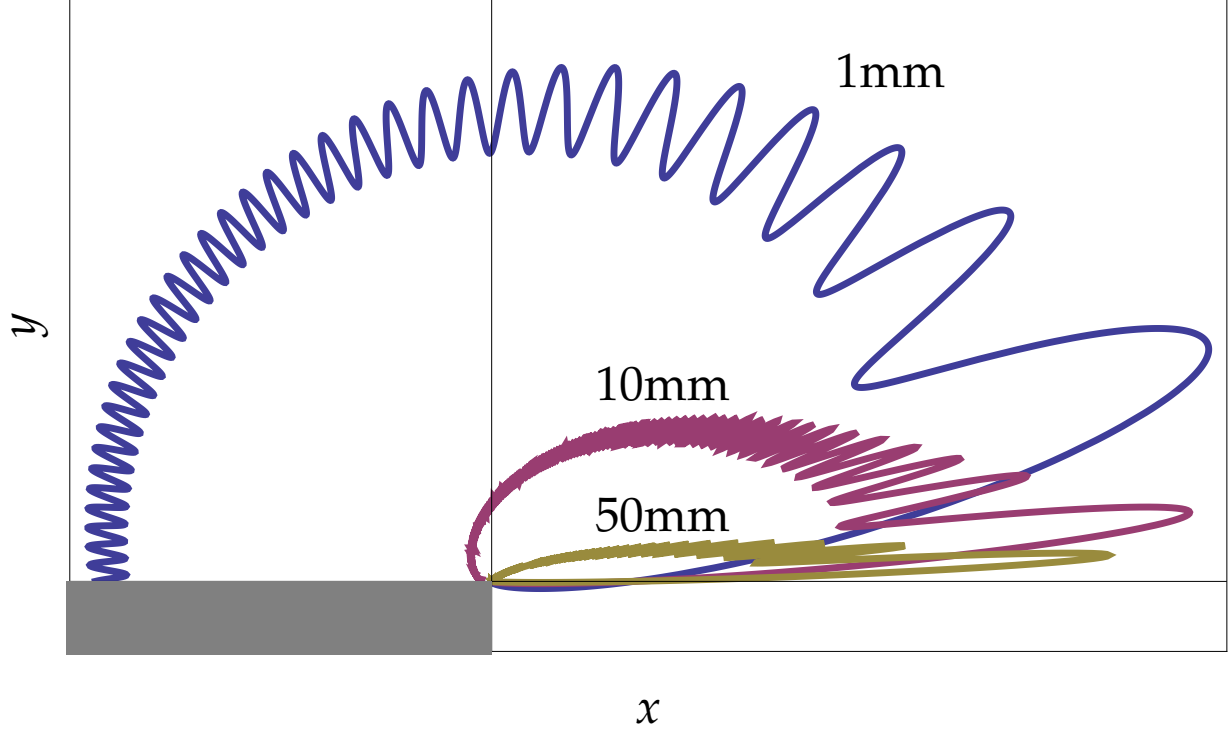


Figure 5. (color online) An angular pattern of a surface wave diffracted by a pure gold wedge for $\lambda = 140 \mu\text{m}$ and $r = 1 \text{ mm}$ (blue), $r = 10 \text{ mm}$ (magenta), and $r = 50 \text{ mm}$ (dark yellow). The x and y axes go along the upper and side faces of the wedge as shown in Fig. 1. The distance to the curve is proportional to the intensity of scattered radiation at the given angle.

in a free space, $r \gg 2\pi/k_0$, both in the near-field and wave zones. The near field was computed numerically in [9, 10] by evaluating the integral in Eq. (14). Eq. (49) gives the desired result with a better accuracy, especially in case where $\text{Im}(\chi_+) \rightarrow 0$.

Angular patterns of diffracted waves computed by formula in Eq. (49) for a pure gold substrate and a gold wedge coated with ZnS film are presented in Figs. 5 and 6, respectively, where the intensity $|B|^2$ is depicted for several distances from the edge of the wedge for parameters relevant to ongoing experiments at Novosibirsk Free Electron Laser. Fig. 5 is typical for the near-field zone, where the angular distribution has many peaks. Fig. 6, on the contrary, shows angular distributions with a single peak characterized by the Lorentzian profile of Eq. (42). In the first case of a pure gold wedge the far wave zone begins after the distance $r \approx 15 \text{ m}$ from the wedge edge whereas for ZnS-coated gold the wave zone is located at $r \approx 20 \text{ mm}$.

In contrast to the Lorentzian profile Eq. (42), the total diffracted field in Eq. (49) is not symmetric about the boundary of the shadow region $\theta \approx -\frac{1}{4}\pi$. It extends into the illuminated region

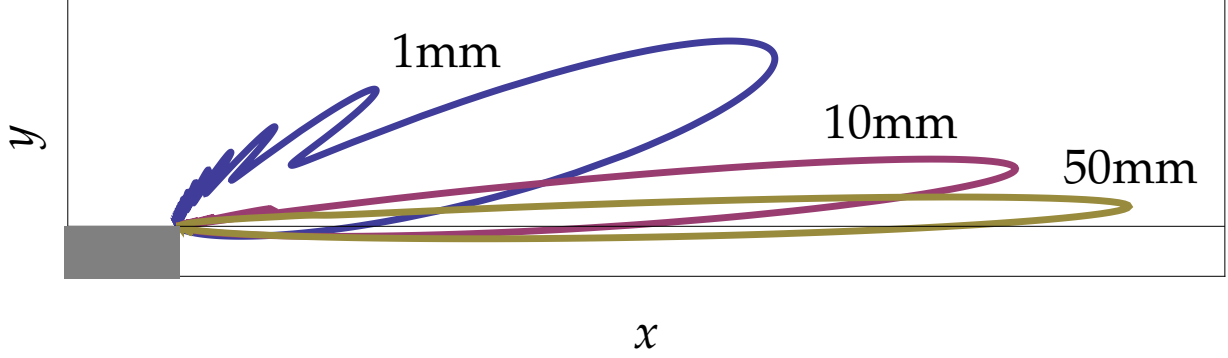


Figure 6. (color online) Same as in Fig. 5 for a gold wedge coated with $0.75\mu\text{m}$ ZnS film: $r = 1\text{ mm}$ (blue), $r = 10\text{ mm}$ (magenta, scaled $\times 4$), $r = 50\text{ mm}$ and (dark yellow, scaled $\times 16$).

$\theta > -\frac{1}{4}\pi$ much further than into the shadow region $\theta < -\frac{1}{4}\pi$. This assertion has found a convincing evidence in experimental data cited in [3]. Another important conclusion is that the radiation intensity in the illuminated area does not copy the profile of the surface wave: instead of monotonic decreasing with the distance from the face of the wedge it rises at first. Again, this fact has been confirmed experimentally [3].

Intensity of diffracted waves vs. distance from the upper face is shown in Figs. 7 and 8, which illustrate that incident surface wave is mainly scattered into the upper hemisphere.

VI. SCATTERED FIELDS NEAR WEDGE FACES

Near the face surfaces of the wedge at $\theta = \pm\frac{3}{4}\pi$ the integrals B_1 and B_2 have commensurate magnitude and both should be computed. Moreover, the integrands in Eqs. (39) obey the equality

$$s(\theta + \pi) = s(\theta - \pi) \quad (50)$$

at $\theta = \pm\frac{3}{4}\pi$ as can be seen from Fig. 3. The approximation of Eq. (45) provides a good fit for the kernel $s(\theta - p)$ near the saddle point $p = -\pi$ for almost entire interval $-\frac{3}{4}\pi < \theta < \frac{3}{4}\pi$ of the angles θ . However it does not satisfy Eq. (50) at the ends and could be improved there.

Near the upper face at $\theta = \frac{3}{4}\pi$ the pole $p_+ = \theta - \chi_+ - \frac{7}{4}\pi$ approaches the saddle point $p = -\pi$ at $\theta = \frac{3}{4}\pi$, as mentioned at the end of Section IV. Expansion of the kernel $s(\theta - p)$ in Eq. (39a) into the Laurent series about the pole $p_+ = \theta - \frac{7}{4}\pi - \chi_+$ near the saddle point $p = -\pi$ has the following form:

$$s(\theta - p) \simeq \frac{1}{3\sqrt{3}} \left(1 + \frac{2\chi_+}{\theta - \frac{7}{4}\pi - \chi_+ - p} \right). \quad (51)$$

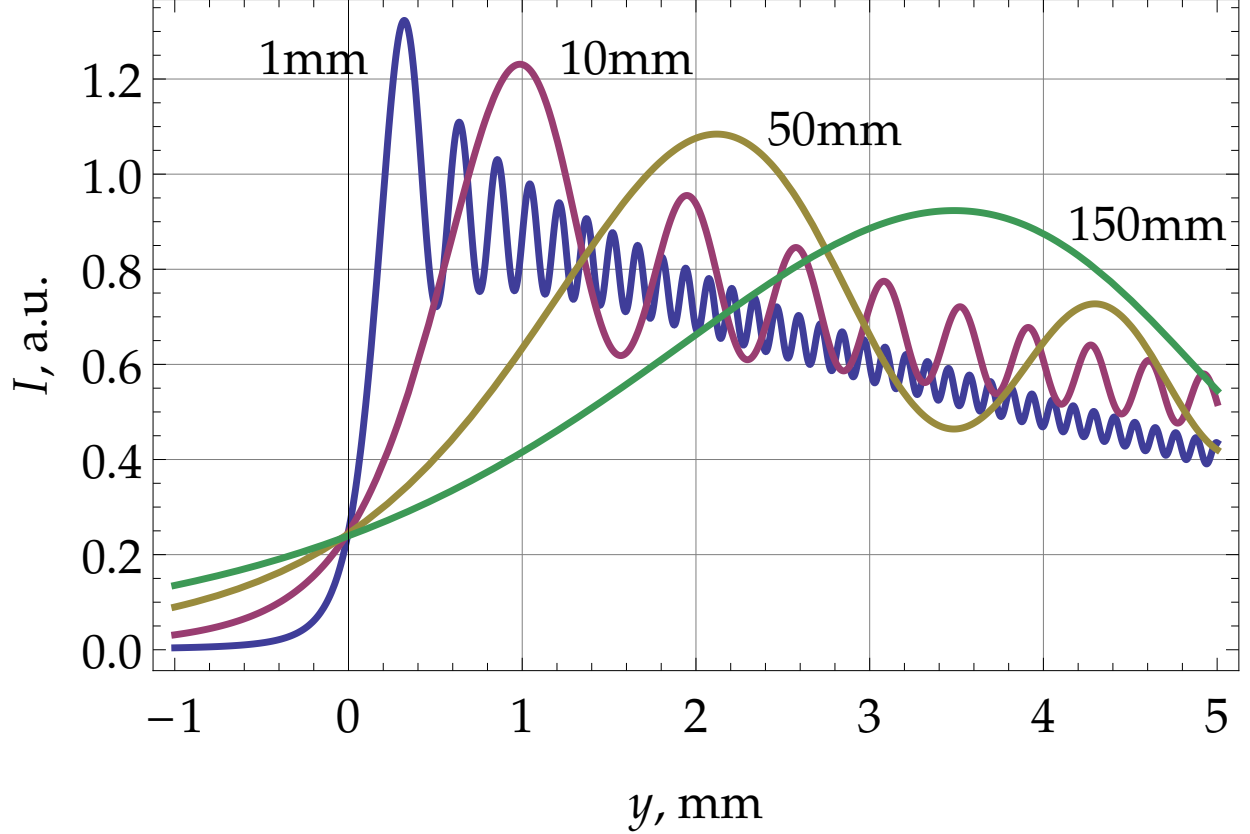


Figure 7. (color online) Intensity of diffracted wave vs. vertical coordinate at different distances from the wedge edge: $x = 1$ mm (blue), $x = 10$ mm (magenta), $x = 50$ mm (dark yellow), and $x = 150$ mm (green). Pure gold wedge.

The kernel

$$s(\theta - p) \simeq -\frac{1}{3\sqrt{3}} \quad (52)$$

in Eq. (39b) is regular at $\theta = \frac{3}{4}\pi$ near the second saddle point $p = \pi$. Combining Eqs. (39), (51), and (52), we obtain

$$\begin{aligned} B_1 + B_2 &\simeq -\frac{1}{2\pi i} \int_{-\infty}^{\infty} \frac{2}{3\sqrt{3}} \left(1 + \frac{\chi_+}{\theta - \frac{3}{4}\pi - \chi_+ - \frac{dp}{dt}t} \right) e^{ik_0r-t^2} \frac{dp}{dt} dt \\ &= \frac{2e^{ik_0r}}{3\sqrt{3}} \left[\frac{e^{i\pi/4}}{\sqrt{2\pi k_0r}} - \chi_+ W_- \left(\frac{1+i}{2} \left(\theta - \frac{3}{4}\pi - \chi_+ \right) \sqrt{k_0r} \right) \right]. \quad (53) \end{aligned}$$

The second term in Eq. (53), containing $\chi_+ W_-$, is small and could be neglected. Eq. (49) gives a similar result at $\theta = \frac{3}{4}\pi$, which differs by a numerical coefficient of the order of unity.

Similarly, the pole $p_- = \theta + \frac{7}{4}\pi + \chi_-$ approaches the saddle point $p = \pi$ at $\theta \rightarrow -\frac{3}{4}\pi$. The

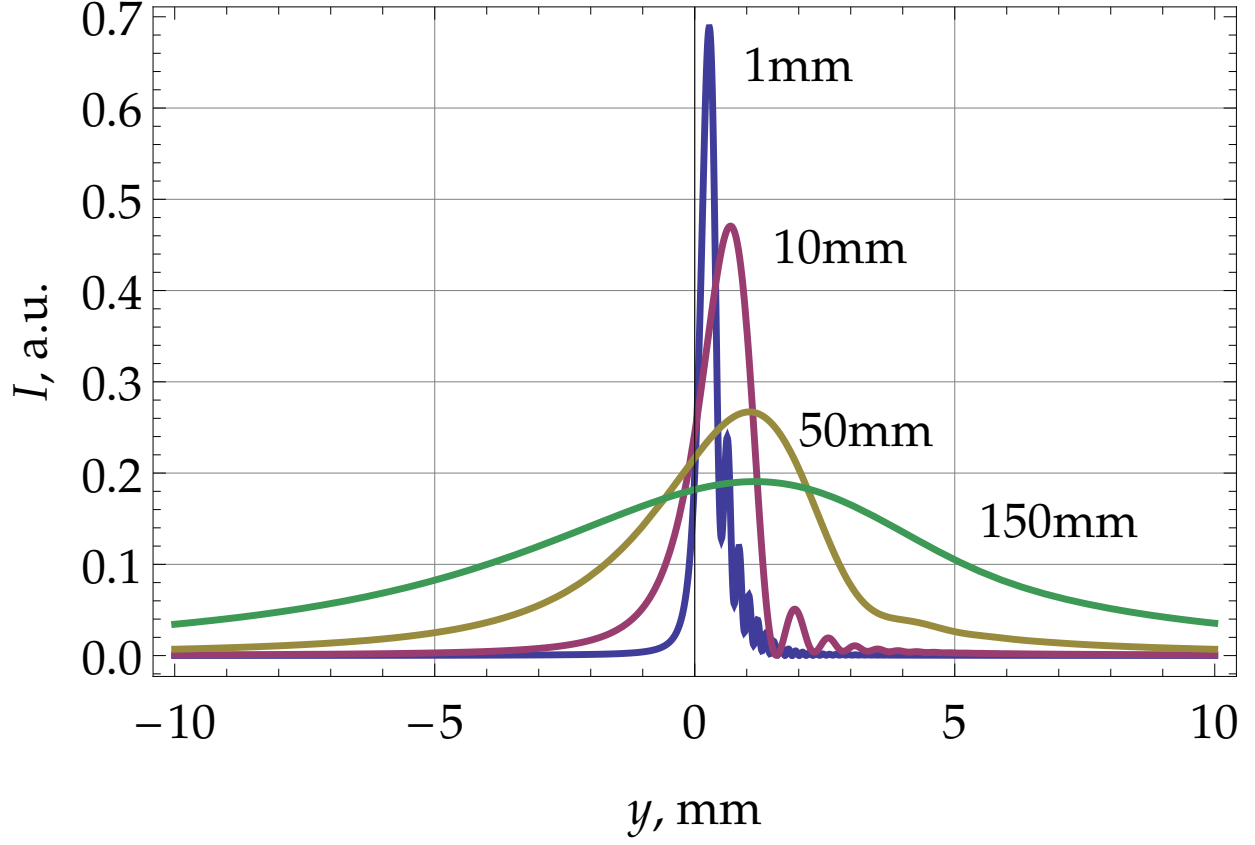


Figure 8. (color online) Intensity of diffracted wave vs. vertical coordinate at different distances from the wedge edge: $x = 1$ mm (blue), $x = 10$ mm (magenta, scaled $\times 2$), $x = 50$ mm (dark yellow, scaled $\times 4$), and $x = 150$ mm (green, scaled $\times 8$). Gold wedge coated with a $0.75\mu\text{m}$ ZnS film.

expansion of the kernel of the integral in Eq. (39b) about p_- has the following form:

$$s(\theta - p) \simeq s_-(\theta - p) = \frac{1}{\sqrt{3}} \left(1 - \frac{2\chi_-}{\theta + \frac{7}{4}\pi + \chi_- - p} \right), \quad (54)$$

and the kernel of Eq. (39a) is

$$s(\theta - p) \simeq -\frac{1}{\sqrt{3}}. \quad (55)$$

Combining Eq. (39) with Eqs. (54) and (55) yields

$$\begin{aligned} B_1 + B_2 &\simeq \frac{1}{2\pi i} \int_{-\infty}^{\infty} \frac{2}{\sqrt{3}} \left(1 - \frac{\chi_-}{\theta + \frac{3}{4}\pi + \chi_- - \frac{dp}{dt}t} \right) e^{ik_0 r - t^2} \frac{dp}{dt} dt \\ &= -\frac{2e^{ik_0 r}}{\sqrt{3}} \left[\frac{e^{i\pi/4}}{\sqrt{2\pi k_0 r}} + \chi_- W_+ \left(\frac{1+i}{2} \left(\theta + \frac{3}{4}\pi + \chi_- \right) \sqrt{k_0 r} \right) \right]. \quad (56) \end{aligned}$$

Again, the second term with χ_- is small and can be dropped.

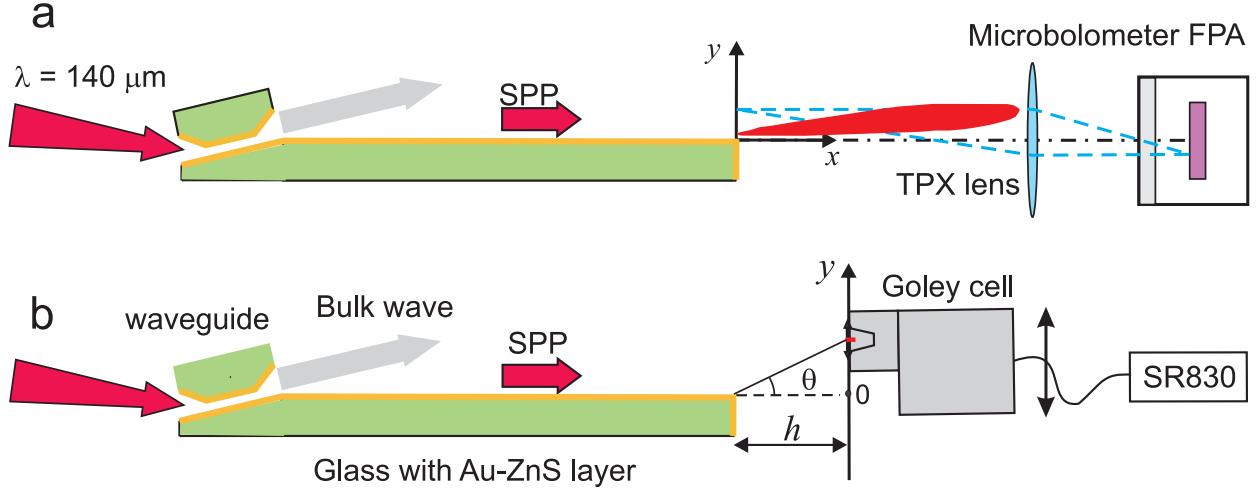


Figure 9. (color online) Experimental configurations for the study of radiation induced by decoupled SPP using (a) a microbolometer focal plane array and (b) a Goley cell coupled to a lock-in amplifier SR830.

Eq. (53) describes a wave propagating along the upper face of the wedge back from the wedge edge, and Eq. (56) is a wave propagating along the lower face. They can be thought of as reflected and refracted waves, respectively, although they are not surface waves. It is interesting that the amplitude of the refracted wave is 3 times larger than the amplitude of the reflected one.

VII. COMPARISON WITH EXPERIMENT

The experimental configurations are shown in Fig. 9. Monochromatic radiation of Novosibirsk Free Electron Laser (FEL) at a frequency of 2.3 THz ($\lambda = 140 \mu\text{m}$) entered the user station through a 16-m long beamline as a Gaussian beam $I = I_0 \exp(-2r^2/w^2)$ with a waist of 9 mm. After passing a circular aperture with a diameter of 10 mm, the beam was focused with a cylindrical mirror into the input mouth of a plane waveguide, formed by the gold-covered facets of two glass prisms. At the output mouth of the waveguide, the radiation passed through the slit, transformed into a surface plasmon-polariton travelling along the metal-dielectric interface. Since a portion of the radiation could be emitted as a free wave, to separate the SPP and the bulk wave we made the input facet of the large prism tapered with an angle of 13 degrees to the upper sample plane. The latter was 17 cm long and 4 cm wide. The edge between these two facets was smoothed for the purpose of decreasing the SPP radiation loss.

The large and small facets of glass slabs were covered with a $1 \mu\text{m}$ thick gold layer, which was considered within this problem as a bulk metal since the skin-depth for the gold is much smaller

than $1\ \mu\text{m}$. The SPPs, which were launched with the help of the waveguide, travelled along the large facet of the samples. Bare gold and gold covered with ZnS layers 0.1 to $3\ \mu\text{m}$ thick were employed in the experiments. To study SPP characteristics we applied two non-invasive techniques for detection of electromagnetic (EM) radiation in the free space behind the end facet of the samples. An optical system consisting of a TPX lens with $f = 50\ \text{mm}$ [30] and a microbolometer focal plane array [31, 32] was used for imaging of the EM radiation wavefronts. Intensity of the EM radiation at different distances h was scanned along the y -axis using an opto-acoustic Goley cell [30] with an input slit $0.2\ \text{mm}$ thick directed along the z -axis.

The experimental results were presented in brief in the conference proceedings [3] and will be published in detail elsewhere [33]. In this paper we present only the data relevant to the contents of the theory, namely we describe characteristics of the electromagnetic field (EMF) that arose when an SPP reached the end of the surface. The main features of the EMF were as follows (see Figs. 10 and 11). (a) The intensity of EMF, in contrast to the SPP intensity, reached its maximum at a distance of 1 to $2\ \text{mm}$ above the sample surface, depending on the ZnS layer thickness, and only then sloped down. (b) Oscillations were observed on the descending part of the distribution. (c) The width of the distribution decreased with the distance and the angular distribution became narrower. All these features are in reasonable agreement with the theoretical predictions. Some discrepancies between the distribution shapes on the slope recorded with the MBFPA and the Goley cell may be caused, for example, by field disturbance by the metal diaphragm at the cell input window.

VIII. CONCLUSIONS

In this paper, we have considered diffraction of a surface wave by a rectangular wedge with impedance facets using the Sommerfeld-Malyuzhinets technique. We have derived Eq. (49) that uniformly describes the diffracted field both in the near-field and far-field zones. It was used in Section V for analysis of diffracted radiation at various distances from the wedge. Main conclusions from this formula are confirmed by available data from ongoing experiments at Novosibirsk Free Electron Laser [3, 33].

First, we have shown that the total diffracted field expressed by Eq. (49) is not symmetric about the boundary of the shadow region and that the surface wave is scattered mainly into the upper hemisphere. It extends into the illuminated region much further than into the shadow region as

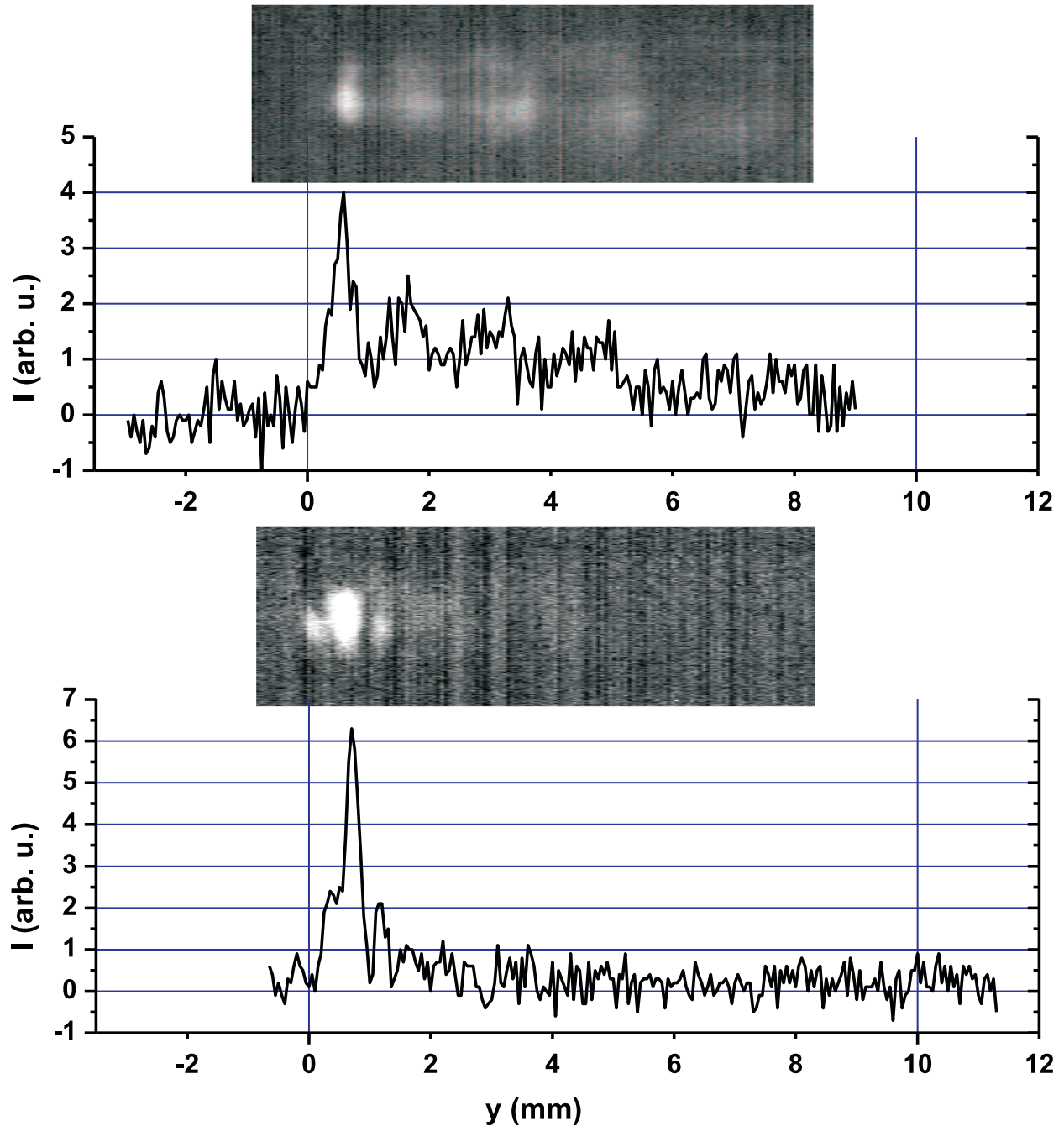


Figure 10. Images of spatial distribution of radiation near the end of a bare gold sample (above) and a sample covered with a 1- μm ZnS layer (below), recorded with the microbolometer focal plane array (configuration of Fig. 9,a).

depicted in Figs. 7 and 8.

Another important conclusion is that the radiation intensity in the illuminated area does not follow a surface wave profile and at first increases instead of monotonic decreasing with the distance

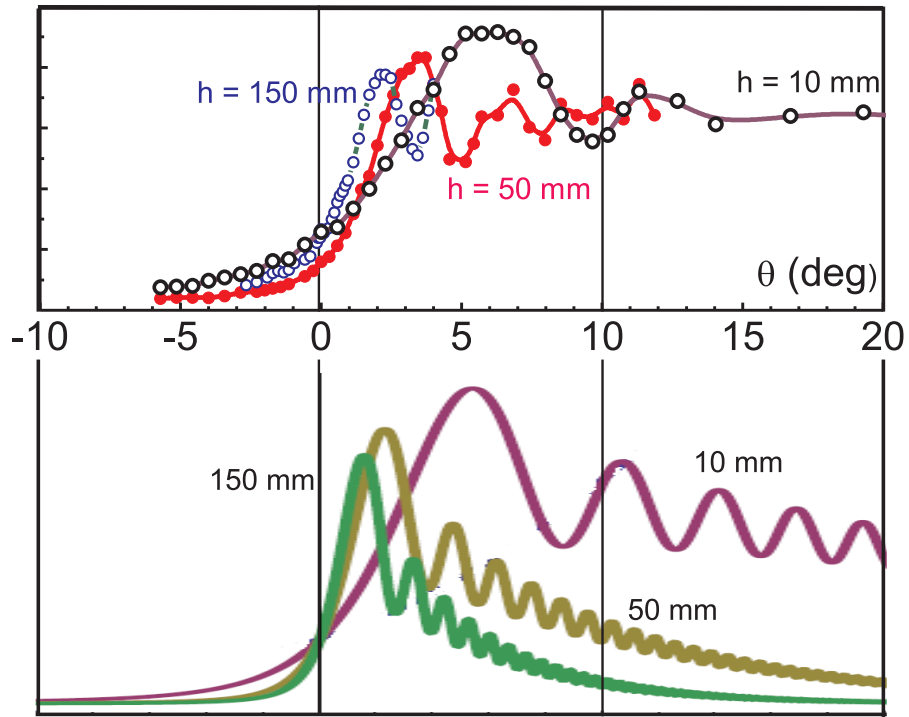


Figure 11. EM wave intensity distribution (in arbitrary units) vs. angle for three distances in the experimental configuration of Fig. 9, b for a bare gold surface: (a) Goley cell signal for three distances from the sample end; (b) simulations.

from the face of the wedge, as one might expect for the surface wave, which exponentially decays with the distance from the metal-air interface. Again, this fact has been confirmed experimentally in [3, 33].

We have confirmed the conclusion made in [9, 10] that in the wave zone the angular distribution of the scattered wave has the Lorentzian form with a width determined by impedance. However, we have noted that the wave zone for a wedge with a small surface impedance begins at very large distances, specified by Eq. (44).

ACKNOWLEDGEMENTS

This work was supported by the Russian Government, grant 11.G34.31.0033, the Russian Foundation for Basic Research, grants 11-02-12252-ofi-m, 11-02-12171-ofi-m , and the Rus-

sian Ministry of Education and Science, state contracts No 14.B37.21.0732, 14.B37.21.0784 and 14.B37.21.0750. The experiments mentioned in the paper were carried out using equipment belonging to the SCSTR.

- [1] S. A. Maier, *Plasmonics: Fundamentals and Applications* (Springer, 2007).
- [2] R. Stanley, *Nature Photonics* **6**, 409 (2012).
- [3] V. V. Gerasimov, V. S. Cherkassky, B. A. Knyazev, I. A. Kotelnikov, A. K. Nikitin, and G. N. Zhizhin, in *37th International Conference on Infrared, Millimeter and Terahertz Waves, September 23-28, 2012. Report Tue-A-4-4* (University of Wollongong, Australia, 2012).
- [4] B. A. Knyazev, G. N. Kulipanov, and N. A. Vinokurov, *Measur. Sci. Techn.* **21**, 054017 (2010).
- [5] V. A. Borovikov and B. Y. Kinber, *Geometrical theory of diffraction*, IEE Electromagnetic Waves Series, Vol. 37 (The Institution of Electrical Engineers, 1994).
- [6] A. Osipov and A. Norris, *Wave Motion* **29**, 313 (1999).
- [7] V. M. Babich, M. A. Lyalinov, and V. E. Grikurov, *Diffraction theory : the Sommerfeld-Malyuzhinets technique*, Alpha Science series on wave phenomena (Alpha Science, Oxford, 2008).
- [8] G. D. Malyuzhinets, *Sov. Phys. Dokl.* **3**, 752 (1959).
- [9] V. B. Zon, *J. Opt. Soc. Am. B* **24**, 1960 (2007).
- [10] V. B. Zon, *J. Opt. A: Pure Appl. Opt.* **9**, 476 (2007).
- [11] N. G. Trenev, *Radiotekh. Elektron.* **3**, 27–37 (1958).
- [12] N. G. Trenev, *Radiotekh. Elektron.* **3**, 163 (1958).
- [13] R. P. Starovoitova, M. S. Bobrovnikov, and V. N. Kislitsina, *Radiotekh. Elektron.* **2**, 250 (1962).
- [14] V. Ivanov, *USSR Computational Mathematics and Mathematical Physics* **10**, 146 (1970).
- [15] V. Ivanov, *USSR Computational Mathematics and Mathematical Physics* **11**, 349 (1971).
- [16] M. Lyalinov, *Radio Science* **31**, 1721 (1996).
- [17] M. A. Lyalinov and N. Y. Zhu, *Wave Motion* **30**, 275 (1999).
- [18] A. Gautesen, *Wave Motion* **41**, 239 (2005), special Issue in Honor of the 75th Birthday of A.T.de Hoop.
- [19] M. A. Lyalinov and N. Y. Zhu, *Wave Motion* **44**, 21 (2006).
- [20] A. Norris and A. Osipov, *Wave Motion* **30**, 69 (1999).

- [21] M. Shimoda, R. Iwaki, M. Miyoshi, and T. Matsuda, *IEICE TRANSACTIONS on Electronics* **7**, 853 (2001).
- [22] V. D. Shafranov, “Electromagnetic waves in a plasma,” in *Reviews of Plasma Physics*, Vol. 3, edited by M. A. Leontovich (Consultants Bureau, New York, 1963) pp. 1–158.
- [23] H. Raether, *Surface Plasmons on Smooth and Rough Surfaces and on Gratings* (Springer-Verlag, New York, 1988).
- [24] V. Klimov, *Nanoplasmonics* (Fizmatlit, Moscow, 2009).
- [25] R. T. Ling, J. D. Scholler, and P. Y. Ufimtsev, *Progress In Electromagnetics Research* **19**, 49 (1998).
- [26] J. F. OHara, W. Withayachumnankul, and I. Al-Naib, *Journal of Infrared, Millimeter and Terahertz Waves* **33**, 245 (2012).
- [27] M. A. Ordal, R. J. Bell, J. R. W. Alexander, L. L. Long, and M. R. Querry, *Applied optics* **24**, 4493 (1985).
- [28] A. Sommerfeld, *Mathematische Annalen* **47**, 317–374 (1896).
- [29] G. D. Maliuzhinets, *Sov. Phys. Dokl.* **3**, 52–56 (1958).
- [30] “<http://www.tydexoptics.com>,” .
- [31] M. A. Dem’yanenko, D. G. Esaev, B. A. Knyazev, G. N. Kulipanov, and N. A. Vinokurov, *Appl. Phys. Lett.* **92**, 131116, 3p. (2008).
- [32] B. A. Knyazev, V. S. Cherkassky, Y. Y. Choporova, V. V. Gerasimov, M. G. Vlasenko, M. A. Dem’yanenko, and D. G. Esaev, *Journal of Infrared, Millimeter, and Terahertz Waves* **32**, 1207 (2011).
- [33] V. V. Gerasimov, V. S. Cherkassky, B. A. Knyazev, I. A. Kotelnikov, A. K. Nikitin, and G. N. Zhizhin, (to be published) (2013).